Titanium Traps

DOI: 10.1002/anie.201310522

Mapping of the Photoinduced Electron Traps in TiO_2 by Picosecond X-ray Absorption Spectroscopy**

*M. Hannelore Rittmann-Frank, Chris J. Milne, Jochen Rittmann, Marco Reinhard, Thomas J. Penfold, and Majed Chergui**

Abstract: *Titanium dioxide (TiO_2) is the most popular material for applications in solar-energy conversion and photocatalysis, both of which rely on the creation, transport, and trapping of charges (holes and electrons). The nature and lifetime of electron traps at room temperature have so far not been elucidated. Herein, we use picosecond X-ray absorption spectroscopy at the Ti K-edge and the Ru L_3-edge to address this issue for photoexcited bare and N719-dye-sensitized anatase and amorphous TiO_2 nanoparticles. Our results show that 100 ps after photoexcitation, the electrons are trapped deep in the defect-rich surface shell in the case of anatase TiO_2, whereas they are inside the bulk in the case of amorphous TiO_2. In the case of dye-sensitized anatase or amorphous TiO_2, the electrons are trapped at the outer surface. Only two traps were identified in all cases, with lifetimes in the range of nanoseconds to tens of nanoseconds.*

Titanium dioxide (TiO_2), in its anatase crystalline form, is the most promising metal-oxide semiconductor for applications in photocatalysis[1] and solar-energy conversion.[2] The band-gap (BG) energy of anatase TiO_2 is 3.2 eV, that is, in a spectral region in which the solar spectrum is weak. To overcome this limitation, sensitization of the TiO_2 substrate by adsorbed dye molecules enables the injection of electrons into its conduction band (CB) upon excitation by visible light.[3] This sensitization, most commonly with ruthenium-based polypyridine complexes, became the basis of dye-sensitized solar cells (DSSCs). The efficiency of photocatalysis and solar-energy conversion depends on the transport and trapping of charge carriers,[1a,4] and although the trapping of electrons in the CB has been known for years,[1,5] the nature of the traps at room temperature remains unknown.

Trapped charges (electron and holes) have been probed by electron paramagnetic resonance (EPR),[1,6] photoluminescence,[5a,7] and O_2 photodesorption.[8] The EPR studies on powdered anatase TiO_2 at 90 K under continuous ultraviolet (UV) irradiation showed two distinct traces attributed to electrons trapped at Ti^{3+} sites that remained unspecified.[6b] However, by IR spectroscopy, it was found that most (about two thirds) of the electrons remain delocalized in the CB as EPR-silent species, even after the discontinuation of UV irradiation. The localized Ti^{3+} traps disappeared above 90 K, whereas EPR-silent traps disappeared above 140 K.[6b]

As far as dye-sensitized anatase TiO_2 is concerned, ultrafast mid-IR absorption studies of electrons injected into the CB of TiO_2 inferred that they randomly populate a small region near the parent adsorbate dye and then relax from the so-called shallow traps to the deep traps, whose structures and energetics are unknown.[9] On the other hand, THz studies suggested that the injected electrons are mobile, because the high dielectric permittivity of TiO_2 efficiently screens the electrostatic interaction between the injected electron and the dye cations.[10] Importantly, whereas UV, visible, infrared, and THz spectroscopic tools are sensitive to free, and probably trapped electrons, they are neither element-specific nor structure-sensitive in the case of the latter.

By X-ray absorption spectroscopy (XAS), X-ray diffraction (XRD), and molecular-dynamics (MD) simulations, it was shown that anatase nanoparticles (NPs) consist of a crystalline core with a substantial contribution of distorted and/or coordination-unsaturated Ti sites at the outer shell[11] owing to truncation of the Ti–O octahedra.[11a,e] The CB of TiO_2 is predominantly composed of Ti (3d) orbitals,[12] and therefore the trapping of electrons at Ti centers may be interrogated by Ti K-edge XAS, which is sensitive to changes in oxidation state and local geometry.[13]

Optical pump/XAS probe techniques with 100 ps resolution were recently implemented in the case of ruthenium[14] and copper[15] dyes adsorbed on TiO_2 to determine the formation and structure of the oxidized dyes at their metal K-edges. However, no probing of the electrons in the TiO_2 substrate was carried out. Previously, Katz et al.[16] reported an Fe K-edge absorption study of iron oxide NPs upon electron injection from adsorbed organic dyes. By comparing their transients with simulated transients, they concluded that the reduced metal sites formed small polarons on a 100 ps time scale. In this study, we used picosecond XAS at the Ti K-edge[17] and the Ru-L_3 edge and visualized the formation of Ti^{3+} electron traps in photoexcited bare and N719-dye-sensitized TiO_2 nanoparticles, along with the formation of the oxidized dye in the latter. We found that beyond 100 ps after the band-gap excitation (at 355 nm) of bare anatase nanoparticles in aqueous solutions, the electrons ended up at two Ti^{3+} trapping sites located deep in the defect-rich surface shell, whereas upon electron injection by excitation of the

[*] Dr. M. H. Rittmann-Frank, Dr. C. J. Milne, Dr. J. Rittmann, Dr. M. Reinhard, Dr. T. J. Penfold, Prof. M. Chergui
Laboratoire de Spectroscopie Ultrarapide, ISIC-FSB
Ecole Polytechnique Fédérale de Lausanne
1015 Lausanne (Switzerland)
E-mail: majed.chergui@epfl.ch
Homepage: http://lsu.epfl.ch/

[**] This research was supported by COST CM0702 (No. SER C08.0101) and by the Swiss NSF through the NCCR-MUST.

Supporting information for this article is available on the WWW under http://dx.doi.org/10.1002/anie.201310522.

sensitizer (at 532 nm), the electrons were trapped at the outer surface.

Figure 1 A shows the steady-state Ti K-edge XAS spectra (see Figure S5 A in the Supporting Information for the full spectra) of colloidal solutions of the 20 nm bare anatase NPs and 10 nm amorphous NPs used in this study (see Figure S1 for their XRD powder patterns). Both sets of data point to striking structural differences at short (XAS) and at long range (XRD). Furthermore, in TEM images (see Figure S2), the anatase NPs exhibited, as expected,[5a] a well-defined shape. The pre-edge XAS region (Figure 1 A) exhibits four peaks, labeled A_{1-3} and B.[11a,f,g,18] The A_2 and A_3 peaks are separated by approximately 1 eV; relative to the A_1 and B peaks they are stronger for the amorphous than for the anatase sample.[11d,e] These peaks are typical of K-shell spectra,[19] that is, transitions from the 1s core orbital to unoccupied Ti 3d valence orbitals. In the regular octahedral Ti^{4+} ($3d^0$) hexacoordinated sites of bulk anatase, these transitions have a quadrupole character, but anatase TiO_2 presents a weak D_{2d} distortion that makes them partially allowed by virtue of 3d/4p mixing, which introduces a dipole component.[13,20] Stronger deviations from octahedral symmetry would further enhance such mixing. The exact assignment of these peaks is still a matter of debate, but there is consensus that A_1 has a predominantly quadrupole character, A_2 and A_3 have a quadrupole + dipole character, and B is predominantly a dipole transition.[11d,e,19–21] The differences between anatase and amorphous NPs suggest different coordination geometries around the Ti atoms.[11f] Furthermore, whereas the A_3 is stronger than the A_2 peak in bulk TiO_2 and in large NPs, the trend is reversed for NPs with diameters less than 5 nm, as the surface-to-volume ratio increases.[11b,d–f] Consequently, the A_2 peak has been attributed a surface character,[11e] but its pronounced presence in bulk amorphous samples may suggest a more specific explanation for its enhanced intensity at the surface. It has also been shown that nonsymmetrically distorted hexacoordinated sites, with an elongated Ti–O bond, can also give rise to a significant enhancement of the A_2 peak.[22] Upon adsorption of the N719 dye, the XAS spectra were unaffected (see Figure S3), whereas the UV/Vis spectra exhibited the additional absorption of the dye in the 400–600 nm region (see Figure S4).

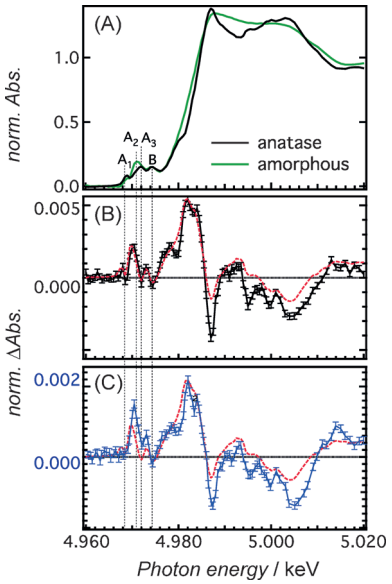

Figure 1. Edge region of XAS spectra of anatase and amorphous TiO_2 NPs (pre-edge peaks A_{1-3} and B, and X-ray absorption near-edge structure). A) Ti K-edge absorption spectra of bare anatase and amorphous TiO_2 NPs. B) Transient X-ray absorption spectra of bare anatase TiO_2 NPs excited at 355 nm at a time delay of 100 ps (black) together with the calculated difference spectrum (red dashed line): the amorphous-sample steady-state spectrum shifted by −1 eV, minus the anatase-sample spectrum (the difference spectrum was scaled by 0.016, by normalization at the edge at 4.982 keV; see text). C) Transient XAS spectrum of N719-dye-sensitized anatase TiO_2 NPs at a time delay of 100 ps (blue) after excitation at 532 nm. The dashed red trace is the same as in (B), but has been scaled by a factor of 0.006.

Figure 1 B shows the transient XAS spectrum (XAS spectrum of the excited sample minus that of the unexcited sample) for bare anatase NPs recorded 100 ps after excitation at 355 nm (see Figure S5 B for the full spectrum). Significant changes observed in the pre-edge, edge, and above-edge regions reflect substantial photoinduced modifications of both the electronic and the geometric structure of Ti centers, which remain unchanged between 100 ps and 1 ns (see Figure S6). Figure 1 C shows the transient spectrum obtained upon the excitation of the dye-sensitized anatase NPs at 532 nm (see Figure S5 C for the full spectrum; the transient spectra obtained upon direct excitation or injection are also compared in Figure S7). Despite similarities, the transient spectrum for dye-sensitized NPs shows stronger A_2/A_3 peaks relative to the main signal at 4.982 keV, as well as significant changes in the above-edge region. We rule out multiphoton excitation at 532 nm above the band gap of dye-sensitized NPs on the basis of the pump-power dependence shown in Figure S8. Furthermore, evidence that the electron is injected from the ruthenium dye upon excitation at 532 nm is provided by a transient spectrum recorded at the Ru L_3-edge (see Figure S9). The derivative-like signal therein reflects the oxidation-state change of the metal from Ru^{2+} to Ru^{3+}, whereas the appearance of a new band at 2837 eV is due to the $2p_{3/2}$–$4d(t_{2g})$ transition. Both observations arise from the creation of a hole in the 4d bonding orbitals upon photo-oxidation of the Ru center.[23]

The transient spectra of bare amorphous (excited at 355 nm) and dye-sensitized amorphous NPs (excited at 532 nm; Figure 2) again show some similarities but also differences in the pre-edge region and between 4.985 and 5.005 keV, as well as in the above-edge region (see inset in Figure 2). Just as for anatase NPs, the changes are more pronounced in the case of the dye-sensitized NPs as compared to the bare NPs.

Figure 3 shows the decay kinetics of the signals at 4.79 (pre-edge), 4.982 (edge), and 5.15 keV for bare and dye-sensitized anatase NPs (see Figures S9 and S10 for the extended time scans). In all cases, the kinetics decay to zero within a few tens of nanoseconds, but more rapidly for bare NPs than for dye-sensitized NPs. However, for a given type of NP, the kinetics are the same to within the error bars at all

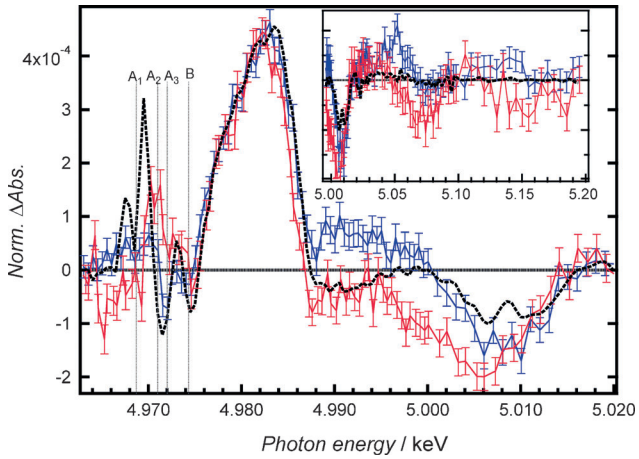

Figure 2. Normalized transient spectra at a time delay of 100 ps of bare amorphous NPs excited at 355 nm (blue) and N719-dye-sensitized amorphous NPs. excited at 532 nm (red). The black dashed line represents the static difference spectrum obtained by subtracting the measured steady-state spectrum from the steady-state spectrum shifted by −1 eV and normalization to the transients at 4.981 keV. The inset shows the above-edge region of the same transient spectra.

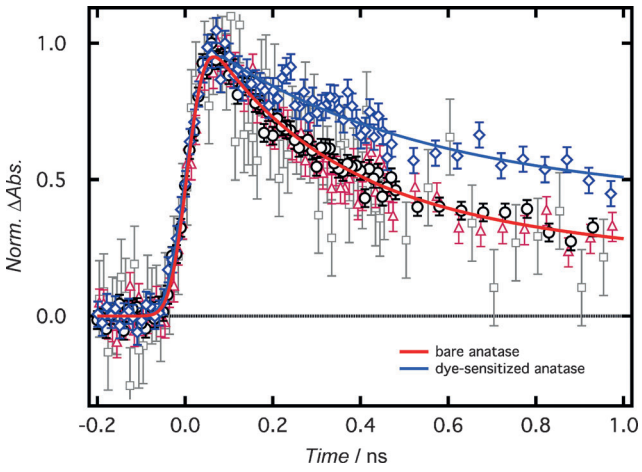

Figure 3. Kinetic traces of the bare anatase nanoparticles as recorded in the pre-edge (4.979 keV, red triangles), the edge (4.982 keV, black circles), and the extended X-ray absorption fine structure (EXAFS; 5.15 keV, gray squares) region and their fit (red line) to a biexponential function with decay time constants of 0.31 and 6 ns (see Table S1 for fit parameters). Blue diamonds show the kinetic trace of dye-coated anatase nanoparticles at 4.982 keV (see Figure S9 B for data for other energies) with a biexponential fit function (blue line) with time constants of 0.5 and 18 ns. The kinetic traces up to 100 ns are shown in Figures S9 and S10 of the Supporting Information.

three energies, thus implying that the changes in the electronic structure (pre-edge and edge region) and the geometric structure (above-edge region) originate from the same species. Figure S12 shows the decay kinetics of the bare and dye-sensitized amorphous NPs. The signals are significantly noisier than for anatase NPs, but again the dye-sensitized samples relax more slowly than the bare samples.

In Figure 1 B (see also Figure S5 B), the maximum transient signal at 4.982 keV occurs just below the edge and is due to its shifting to lower energies by 0.5 to 1 eV as a result of the reduction of Ti^{4+} to Ti^{3+}.[24] The pre-edge bands undergo a similar shift (Figure 1 B). They exhibit an enhancement of the A_2/A_3 bands, which are prominent in amorphous NPs (Figure 1 A). Finally, the changes in the above-edge region are mostly due to the amplitude reduction of the features at 4.987, 5.005, 5.07, and 5.15 keV (highlighted by vertical lines in Figure S5), all of which are clear in anatase NPs but are weak or missing in amorphous NPs (Figure 1 A; see also Figure S5 A). These observations hint at the idea that photoexcitation induces a shift of spectral weight from the anatase features to amorphous-like features. As a matter of fact, we could reproduce the transient spectra (Figure 1 B,C; see also Figure S5 B,C) by taking the scaled difference between the amorphous static spectrum shifted by −0.5 to −1 eV (due to the oxidation shift) and the anatase static spectrum (see Figure S14). The result is shown as dashed traces in Figure 1 (and Figure S5). The scaling was carried out by normalizing the static difference and the transient spectra at the maximum (i.e. at the edge) with the scaling factors as adjustable parameters. These parameters are 0.016 and 0.006 for bare NPs and dye-sensitized NPs, respectively. They reflect the population yield of Ti^{3+} sites 100 ps after electron delivery to the CB (excitation or injection) under our experimental conditions. For bare NPs (Figure 1 B; see also Figure S5 B), we found a very good agreement between the scaled difference and the transient spectrum, in particular in the pre-edge region. There are also some weak deviations, most notably in the edge region (between 4.983 and 5.020 keV), which are probably due to structural rearrangements at traps upon the reduction of Ti^{4+} to Ti^{3+}. The static difference of the shifted anatase spectrum minus itself yields a poor agreement with the experimental data, regardless of the shift (see Figure S14). For the dye-sensitized NPs (Figure 1 C; see also Figure S5 C), the agreement is satisfactory, but not as good as for bare NPs, in line with the overall more pronounced changes in these NPs (see Figure S7).

The agreement between the scaled static difference spectrum and the transient spectrum suggests that in both bare and dye-sensitized anatase NPs, the electrons delivered to the CB end up in pre-existing "amorphous-like" trapping sites, which are mostly found in the outer shell of anatase NPs.[11c,e,25] We therefore conclude that after excitation, part of the electrons migrate to the defect-rich surface shell and get trapped there. Although trapping sites may also occur within the anatase core, Figure 1 A (as well as Figures S1 and S15) shows that this possibility is unlikely. The shift of spectral weight to "amorphous-like" trapping sites at the expense of regular anatase sites is clearly not due to a structural phase transition, since the kinetics decay to zero (see Figures S10 and S11), and the samples are photostable (see the Supporting Information). In the case of dye-sensitized NPs, the electron is delivered to the outer surface. Interestingly, the surface-specific A_2 feature[11e] in Figure 1 C is enhanced as compared to that in Figure 1 B, thus suggesting that the electron is trapped at or in the immediate vicinity of the surface, whereas for bare anatase NPs, the very good agreement between the

scaled difference spectrum and the transient spectrum implies that the electron is trapped deeper inside the defect-rich surface shell, that is, at subsurface traps.

In the case of amorphous NPs (Figure 2), the transient spectra can be well reproduced by taking the difference between the static spectrum shifted by approximately −1 eV and the unshifted spectrum; that is, the strongest changes are caused by the oxidation-state shift, thus implying that electron localization occurs inside the NP. In the above-edge region (see inset), the agreement is somewhat better for bare NPs than for sensitized NPs. The deviations therein are due to the fact that upon reduction to Ti^{3+}, the pre-existing defects undergo structural changes, which are neglected in the static difference spectrum. In the pre-edge region, deviations appear again because the occupancy of Ti (3d) orbitals upon reduction is also neglected in the static difference spectrum. In the case of the dye-sensitized NPs, and just as for the anatase NPs, the A_2 feature is enhanced, thus highlighting the fact that the electron is trapped at or in the vicinity of the surface. This result also suggests that the surface traps of amorphous NPs are similar to those of anatase NPs.

The kinetic traces for bare anatase NPs (Figure 3) can be equally well fitted by using bi- or triexponential functions convoluted to the 70 ps X-ray pulse width, but not a stretched exponential (see Figure S11 B). The kinetic traces of the dye-sensitized anatase NPs and the bare amorphous NPs are best fitted by a biexponential function (see Figure S12). Finally, for the dye-sensitized amorphous NPs, no fit was attempted owing to the poor signal-to-noise ratio. The good agreement between the fit parameters for bare anatase and amorphous NPs (see Table S1) supports the "amorphous" character of the trapping sites in anatase NPs, as already highlighted in Figure 1 B (see also Figure S5 B). Furthermore, it points to the biexponential fit as the most likely for anatase NPs. For the dye-sensitized anatase NPs, both components become significantly larger, compared to those for the bare NPs, and the pre-exponential factor of the long component increases relative to that of the short component. Therefore, in spite of the fact that the electron is trapped at the surface with the adsorbed dye on it, its lifetime is longer than in bare NPs. Finally, the rise of the signal is X-ray-pulse-limited, thus implying that the traps are populated within 70 ps in all cases, in bare or dye-sensitized NPs. This behavior is in line with previous reports of an approximately 250 fs[26] electron-trapping time.

In the following, we distinguish between subsurface (BG excitation) and surface traps (injection). The biexponential nature of the subsurface-trap decay supports the existence of two Ti^{3+} trap states, in agreement with low-temperature EPR studies,[6b] but in this study, we observed them at room temperature and determined their lifetimes (see Table S1). However, given that we mainly identified the traps on the basis of enhancements of the A_2/A_3 bands, we can only speculate about their geometry. Indeed, any deviation of the trap symmetry from octahedral to distorted hexacoordinated or pentacoordinated sites (square-pyramidal C_{4v} or trigonal bipyramidal D_{3h} sites) or tetracoordinated sites (T_d symmetry) would lead to increased 3d/4p mixing, which would enhance the intensity of the A_2/A_3 bands. The most likely sites for the subsurface traps may well be nonsymmetrically distorted hexacoordinated and pentacoordinated sites. However, at this point it is difficult to determine which of the two is the energetically deeper trap. Furthermore, although our measurements are only sensitive to trapping beyond 100 ps, it is very likely that several energetically "shallow" traps are visited at earlier times.[1b] It is remarkable that for amorphous NPs excited above the band gap, although a larger distribution of trap geometries is in principle available, the kinetics also point to two sites at ≥ 100 ps; these two sites, judging from the decay times, seem to be identical to those of anatase NPs.

As far as surface trapping is concerned, Ti–OH groups have been proposed to play an important role, with the formation of Ti^{3+}–OH.[27] Density functional theory (DFT) on hydroxylated and reduced rutile TiO_2 (110) surfaces[28] demonstrated the electron-trapping nature of bridging Ti–OH groups. The excess electrons at the hydroxylated surface are trapped at two types of sites: a sixfold-coordinated Ti site located between two bridging hydroxy groups, with an energy of 1.6 eV below the conduction band, and a fivefold-coordinated Ti site, with an energy 1.2 eV below the conduction band. These two energetically stable traps would be related to the two decay components that we found. Because they are located at the surface, the geometry of these traps is more sharply defined than deeper in the shell, which explains the stronger deviations between the scaled difference and transient spectra (Figure 1 C; see also Figure S5 C). Although the distance to the cation is not known, the existence of surface trapped electrons lends support to the hypothesis of an intermediate electron–cation complex.[9,10]

The longer electron lifetimes in dye-sensitized NPs are advantageous for photocatalysis, but not for solar-energy conversion, either by DSSCs or by newly developed perovskite-based solar cells.[29] In such solar cells, interfacial effects are crucial.

Received: December 4, 2013
Revised: April 3, 2014
Published online: May 12, 2014

Keywords: dye-sensitized solar cells · electron trapping · photocatalysis · titanium dioxide · X-ray absorption spectroscopy

[1] a) A. L. Linsebigler, G. Q. Lu, J. T. Yates, *Chem. Rev.* **1995**, *95*, 735–758; b) A. Fujishima, X. T. Zhang, D. A. Tryk, *Surf. Sci. Rep.* **2008**, *63*, 515–582.
[2] a) B. O'Regan, M. Grätzel, *Nature* **1991**, *353*, 737–740; b) I. Chung, B. Lee, J. Q. He, R. P. H. Chang, M. G. Kanatzidis, *Nature* **2012**, *485*, 486–494.
[3] M. K. Nazeeruddin, E. Baranoff, M. Grätzel, *Solar Energy* **2011**, *85*, 1172–1178.
[4] M. R. Hoffmann, S. T. Martin, W. Y. Choi, D. W. Bahnemann, *Chem. Rev.* **1995**, *95*, 69–96.
[5] a) C. C. Mercado, F. J. Knorr, J. L. McHale, S. M. Usmani, A. S. Ichimura, L. V. Saraf, *J. Phys. Chem. C* **2012**, *116*, 10796–10804; b) K. Fujihara, S. Izumi, T. Ohno, M. Matsumura, *J. Photochem. Photobiol. A* **2000**, *132*, 99–104; c) F. J. Knorr, D. Zhang, J. L. McHale, *Langmuir* **2007**, *23*, 8686–8690.

[6] a) N. M. Dimitrijevic, Z. V. Saponjic, B. M. Rabatic, O. G. Poluektov, T. Rajh, *J. Phys. Chem. C* **2007**, *111*, 14597 – 14601; b) T. Berger, M. Sterrer, O. Diwald, E. Knözinger, D. Panayotov, T. L. Thompson, J. T. Yates, *J. Phys. Chem. B* **2005**, *109*, 6061 – 6068.
[7] Y. Yamada, Y. Kanemitsu, *Appl. Phys. Lett.* **2012**, *101*, 133907.
[8] T. L. Thompson, J. T. Yates, *J. Phys. Chem. B* **2005**, *109*, 18230 – 18236.
[9] a) H. N. Ghosh, J. B. Asbury, T. Q. Lian, *J. Phys. Chem. B* **1998**, *102*, 6482 – 6486; b) Y. X. Weng, Y. Q. Wang, J. B. Asbury, H. N. Ghosh, T. Q. Lian, *J. Phys. Chem. B* **2000**, *104*, 93 – 104; c) Y. Tachibana, S. A. Haque, I. P. Mercer, J. R. Durrant, D. R. Klug, *J. Phys. Chem. B* **2000**, *104*, 1198 – 1205.
[10] H. Němec, J. Rochford, O. Taratula, E. Galoppini, P. Kužel, T. Polívka, A. Yartsev, V. Sundström, *Phys. Rev. Lett.* **2010**, *104*, 197401.
[11] a) V. Luca, S. Djajanti, R. F. Howe, *J. Phys. Chem. B* **1998**, *102*, 10650 – 10657; b) L. X. Chen, T. Rajh, Z. Y. Wang, M. C. Thurnauer, *J. Phys. Chem. B* **1997**, *101*, 10688 – 10697; c) P. K. Naicker, P. T. Cummings, H. Z. Zhang, J. F. Banfield, *J. Phys. Chem. B* **2005**, *109*, 15243 – 15249; d) H. Z. Zhang, B. Chen, J. F. Banfield, G. A. Waychunas, *Phys. Rev. B* **2008**, *78*, 214106; e) V. Luca, *J. Phys. Chem. C* **2009**, *113*, 6367 – 6380; f) T. L. Hanley, V. Luca, I. Pickering, R. F. Howe, *J. Phys. Chem. B* **2002**, *106*, 1153 – 1160; g) T. Rajh, J. M. Nedeljkovic, L. X. Chen, O. Poluektov, M. C. Thurnauer, *J. Phys. Chem. B* **1999**, *103*, 3515 – 3519.
[12] R. Asahi, Y. Taga, W. Mannstadt, A. J. Freeman, *Phys. Rev. B* **2000**, *61*, 7459 – 7465.
[13] F. Farges, G. E. Brown, J. J. Rehr, *Phys. Rev. B* **1997**, *56*, 1809 – 1819.
[14] X. Y. Zhang, G. Smolentsev, J. C. Guo, K. Attenkofer, C. Kurtz, G. Jennings, J. V. Lockard, A. B. Stickrath, L. X. Chen, *J. Phys. Chem. Lett.* **2011**, *2*, 628 – 632.
[15] J. Huang, O. Buyukcakir, M. W. Mara, A. Coskun, N. M. Dimitrijevic, G. Barin, O. Kokhan, A. B. Stickrath, R. Ruppert, D. M. Tiede, J. F. Stoddart, J.-P. Sauvage, L. X. Chen, *Angew. Chem.* **2012**, *124*, 12883 – 12887; *Angew. Chem. Int. Ed.* **2012**, *51*, 12711 – 12715.
[16] J. E. Katz, X. Y. Zhang, K. Attenkofer, K. W. Chapman, C. Frandsen, P. Zarzycki, K. M. Rosso, R. W. Falcone, G. A. Waychunas, B. Gilbert, *Science* **2012**, *337*, 1200 – 1203.
[17] F. A. Lima, C. J. Milne, D. C. V. Amarasinghe, M. H. Rittmann-Frank, R. M. van der Veen, M. Reinhard, V. T. Pham, S. Karlsson, S. L. Johnson, D. Grolimund, C. Borca, T. Huthwelker, M. Janousch, F. van Mourik, R. Abela, M. Chergui, *Rev. Sci. Instrum.* **2011**, *82*, 063111.
[18] a) L. X. Chen, T. Rajh, W. Jager, J. Nedeljkovic, M. C. Thurnauer, *J. Synchrotron Radiat.* **1999**, *6*, 445 – 447; b) P. C. Angelome, L. Andrini, M. E. Calvo, F. G. Requejo, S. A. Bilmes, G. J. A. A. Soler-Illia, *J. Phys. Chem. C* **2007**, *111*, 10886 – 10893.
[19] T. Yamamoto, *X-Ray Spectrom.* **2008**, *37*, 572 – 584.
[20] T. Uozumi, K. Okada, A. Kotani, O. Durmeyer, J. P. Kappler, E. Beaurepaire, J. C. Parlebas, *Europhys. Lett.* **1992**, *18*, 85 – 90.
[21] K. E. Lee, M. A. Gomez, T. Regier, Y. F. Hu, G. P. Demopoulos, *J. Phys. Chem. C* **2011**, *115*, 5692 – 5707.
[22] N. Jiang, D. Su, J. C. H. Spence, *Phys. Rev. B* **2007**, *76*, 214117.
[23] W. Gawelda, M. Johnson, F. M. F. de Groot, R. Abela, C. Bressler, M. Chergui, *J. Am. Chem. Soc.* **2006**, *128*, 5001 – 5009.
[24] F. M. F. de Groot, Z. W. Hu, M. F. Lopez, G. Kaindl, F. Guillot, M. Tronc, *J. Chem. Phys.* **1994**, *101*, 6570 – 6576.
[25] S. H. Szczepankiewicz, J. A. Moss, M. R. Hoffmann, *J. Phys. Chem. B* **2002**, *106*, 2922 – 2927.
[26] X. J. Yang, N. Tamai, *Phys. Chem. Chem. Phys.* **2001**, *3*, 3393 – 3398.
[27] S. H. Szczepankiewicz, A. J. Colussi, M. R. Hoffmann, *J. Phys. Chem. B* **2000**, *104*, 9842 – 9850.
[28] C. Di Valentin, G. Pacchioni, A. Selloni, *Phys. Rev. Lett.* **2006**, *97*, 166803.
[29] H. J. Snaith, *J. Phys. Chem. Lett.* **2013**, *4*, 3623 – 3630.

